Macrothink Institute™

Environmental Management and Sustainable Development
ISSN 2164-7682
2016, Vol. 5, No. 2

Flight Considerations and Hyperspectral Image Classifications for Dryland Vegetation Management from a Fixed-wing UAS

Jessica J. Mitchell (Corresponding author)

Department of Geography and Planning, Appalachian State University

PO Box 32066, Boone, NC 28606, USA

Tel: 1-828-262-7054 E-mail: mitchelljj@appstate.edu

Nancy F. Glenn

Boise Center Aerospace Lab, Department of Geosciences, Boise State University

1901 University Drive, Boise ID 83725-1535, USA

E-mail: nancyglenn@boisestate.edu

Matthew O. Anderson and Ryan Hruska

Idaho National Laboratory, 2525 North Fremont Ave, Idaho Falls, ID, USA

E-mail: Matthew.Anderson@inl.gov, Ryan.Hruska@inl.gov

Received: April 20, 2016 Accepted: May 7, 2016

doi:10.5296/emsd.v5i2.9343 URL: http://dx.doi.org/10.5296/emsd.v5i2.9343

Abstract

Unmanned Aerial Systems (UAS)-based hyperspectral remote sensing capabilities developed by the Idaho National Lab and Boise Center Aerospace Lab were tested via demonstration flights that explored the influence of altitude on geometric error, image mosaicking, and dryland vegetation classification. The motivation for this study was to better understand the challenges associated with UAS-based hyperspectral data for distinguishing native grasses such as Sandberg bluegrass (*Poa secunda*) from invasives such as burr buttercup (*Ranunculus testiculatus)* in a shrubland environment. The test flights successfully acquired usable flightline data capable of supporting classifiable composite images. Unsupervised

classification results support vegetation management objectives that rely on mapping shrub cover and distribution patterns. However, supervised classifications performed poorly despite spectral separability in the image-derived endmember pixels. In many cases, the supervised classifications accentuated noise or features in the mosaic that were artifacts of color balancing and feathering in areas of flightline overlap. Future UAS flight missions that optimize flight planning; minimize illumination differences between flightlines; and leverage ground reference data and time series analysis should be able to effectively distinguish native grasses such as Sandberg bluegrass from burr buttercup.

Keywords: Unmanned, Fixed-wing; drones, Imaging spectroscopy, Vegetation, Management, Sagebrush, Monitoring, Hyperspectral

1. Introduction

A growing number of imaging systems are being deployed on various UAS platforms for agricultural, forested and rangeland applications. Recent agricultural investigations have estimated biophysical and biochemical parameters (e.g., LAI, water stress, chlorophyll, fluorescence) by combining lightweight hyperspectral sensors that sample across narrow, near-contiguous wavelengths in portions of the visible near infrared (VNIR, 400 – 1100 nm) with either fixed-wing (e.g., Duan et al, 2014; Zarco-Tejada et al 2013) or rotor-based platforms (Suomalainen et al, 2014; Uto et al, 2013). Lucieer et al (2014) recently demonstrated the use of a rotor-based pushbroom hyperspectral sensor system to generate vegetation maps such as chlorphyll content, leaf area index (LAI) and plant vigour over agricultural lands and Antartic ecosystems. Additional recent rotor-based studies have demonstrated the use of discrete return lidar (Wallace et al, 2014) and 3 dimensional point clouds generated from digital images for forest inventory applications (Puliti et al, 2015). Lightweight, fixed-wing UAS platforms have also been used for characterizing and monitoring forested and dryland vegetation, but primarily in combination with still-cameras or multispectral payloads (e.g., Hardin et al, 2005; Laliberte and Rango, 2009; Michez et al, 2016). While registering and mosaicking a large volume of individual photos with high percent overlap can be challenging (Hardin et al, 2011), automated workflows have been developed to address these issues (Laliberte et al, 2011). Fixed-wing systems tend to have longer flight times than smaller rotor-based platforms; however, they also face unique flight stability and engine vibration challenges (Anderson and Gaston, 2013; Hruska et al., 2012).

In this study we demonstrate how combining a lightweight, fixed-wing aircraft with a VNIR hyperspectral sensor offers new opportunities in remote sensing for applications amenable to belt transect sampling or small project area mosaics (4 to 10 km^2) at the sub-meter to meter pixel resolution. These collection systems span the gap between sampling on the ground and sampling from larger fixed-winged platforms (manned or unmanned) that operate at relatively higher altitudes and collect hyperspectral imagery at resolutions on the order of two to five meters. The fixed-wing UAS system in this study is capable of providing on-demand, repeat hyperspectral acquisitions for durations of approximately 12 hours. The configuration is a cost-effective alternative to more expensive hyperspectral airborne acquisitions and can repeatedly collect imagery throughout a growing season at a spatial resolution uniquely suited

for characterizing complex dryland ecosystems (e.g, Hardin et al, 2005; Laliberte and Rango 2009). These environments are typically highly heterogeneous and composed of mixed target signals that are difficult to unmix in traditional airborne hyperspectral imagery (e.g., Mitchell et al, 2009; Okin et al, 2011).

UAS capabilities had been routinely refined via tests flights conducted at a runway and research park in southeastern Idaho, USA (Hruska et al, 2012), and at the Orchard Training Area (OTA) in southwestern Idaho, USA. Field data collection and image processing tasks for sensor characterization and demonstration of vegetation monitoring applications have accompanied these test flights and this study is a continuation of work presented in Hruska et al (2012). UAS-based hyperspectral flights conducted at OTA in May, 2011tested the extent to which increased flight altitude could improve image mosaicking, and effectively discriminate among non-vegetation targets, grasses and shrubs. Up until the 2011 OTA flights, altitude restrictions contributed to pixel distortion and incomplete coverage, which prevented effective mosaicking and classification. This paper presents realistically achievable dryland ecosystem classification results in the context of vegetation management and restoration monitoring applications.

2. Methods

A series of demonstration flights and ground reference data collections were completed across an area of land within a 4-km radius of the Range 03 runway at OTA, near Boise, Idaho, USA, from 09 May to 12 May 2011. Data collection was conducted in cooperation with the Idaho Army National Guard and the Bureau of Land Management (BLM). The OTA is an Army National Guard joint military installation (57,996 hectares) located within the Snake River Birds of Prey National Conservation Area (NCA). The BLM is interested in prioritizing and monitoring restoration projects across the NCA within the context of ecosystem resiliency. Remote sensing monitoring components include relationships between the spatial arrangement of shrubs and disturbance gradients, vegetation cover and species composition, and native and non-native species distribution patterns.

2.1 UAS Data Collection

The complete UAS-based hyperspectral collection system consists of a PIKA II imaging spectrometer and P-CAQ airborne data acquisition unit (Resonon, Inc., Bozeman, MT); a Piccolo II autopilot (Cloud Cap Technology, Hood River, OR); and a medium altitude long endurance (over 12 hours) Arcturus T-16 airframe, which is designed to carry payloads weighing up to 8 kg in a 12,000 cm^3 payload compartment (Arcturus UAS, Rohnert Park, CA). The PIKA II sensor is a visible/near-infrared pushbroom system configurable up to 240 bands across the 400 nm to 900 nm spectral range, with a maximum spectral resolution of 2.1 nm.

Earlier flights conducted at altitudes under 350 m AGL tended to exacerbate flight instability and the pixel size (under 29 x 29 cm) was considered too small to absorb high frequency error that was evident in the imagery. In addition, narrow flightlines with minimal overlap resulted in significant data gaps that precluded mosaicking the flightlines into a single image

that could be classified. By evaluating scan-line to scan-line error and pixel distortion in the original imagery, it was determined that coarsening the pixel resolution to 1.1 m should be sufficient to absorb high frequency error in the imagery. On 11 May 2011, a full-coverage PIKA II dataset was collected over the project area at a flight altitude of 1676 m above ground level (AGL), which resulted in a nominal square pixel resolution of 1.1 m (Figure 1) (Hruska et al, 2012). Flightlines generated a swath width of 352 m and 50% side overlap was specified. The sensor was configured with 320 cross track pixels and 80 channels, with a spectral resolution of 6.3 nm. Additional flight configurations are the same as those presented in Hruska et al (2012). In addition to the hyperspectral overflights, an ultra-high spatial resolution (4.2 cm square pixel resolution) true color digital camera, Rapid Airfield Damage Assessment System (RADAS), was deployed from a second Arcturus T-16 airframe on 12 May 2011 to support vegetation mapping efforts. Photos were acquired for roughly 40% of the study, then cancelled due to a lens aperture malfunction.

2.2 Field Data Collection

During the week of overflights, ground reference data were collected throughout the project area using WAAS-enabled Trimble GeoXT (Sunnyvale, California) model GPS receiver with real-time corrections for submeter positional accuracy. Ground control points were collected throughout the project area, as well as polygon training data for several dense, homogenous stands of sagebrush (*Artemisia tridentata*; ARTR), Sandberg bluegrass (*Poa secunda*; POSE), bur buttercup (*Ranunculus testiculatus*; RATE), and "slickspots". Slickspots are small, distinct ground patches characterized by a clay subsurface soil horizon and which can host the sensitive vegetation species slickspot peppergrass (*Lepidium papilliferum*). In addition to training polygons, 60 random categorical cover plots (1 m X 1 m) were collected throughout the project area using a random sampling scheme stratified by shrub and non-shrub regions obtained from a year 2000 Landsat-based cover classification developed by the Environmental Management Office of the State of Idaho Military Division. Each of the 60 plots was divided into four quadrats and cover was estimated on the basis of target presence or absence in each quadrat, where target presence in any one quadrat equated to 25% canopy cover. Target categories consisted of shrub, herbaceous and bare ground.

Absolute reflectance measurements (350–2500 nm) were collected on the ground, in the vicinity of the runway, using a FieldSpec® Pro spectroradiometer (Analytical Spectral Devices Inc., Boulder, CO, USA). Targets included barge ground; sagebrush, rabbitbrush (*Chrysothamnus* spp.), burr buttercup and Sandberg bluegrass. A series of four measurements (15 replicates per measurement) were made holding a bare fibre tip (25◦) at waist height, which equates to a field of view approximately 11–18 cm in diameter. Reflectance was calibrated between samples using a white spectralon panel (Labsphere Inc., North Sutton, NH, USA) and collection was limited to within 2 hours of solar noon under clear-sky conditions.

2.3 Hyperspectral Data Processing

Radiometric and geometric corrections were applied to individual flightlines using GeoReg post-processing geocorrection software (Space Computer Corporation, Los Angeles, CA, USA) provided by the PIKA II vendor. The GeoReg software is specifically developed to

radiometrically correct and georegister flightlines obtained by Resonon's pushbroom hyperspectral sensor. GeoReg software was used to convert raw digital numbers collected at the sensor to radiance using lab-derived radiometric calibration coefficients. Individual flightlines were then atmospherically corrected (Fast Line-of-sight Atmospheric Analysis of Spectral Hypercubes or FLAASH), mosaicked, and classified using Environment for Visualizing Images (ENVI) version 4.8 software (ExelisVIS, Boulder, CO).

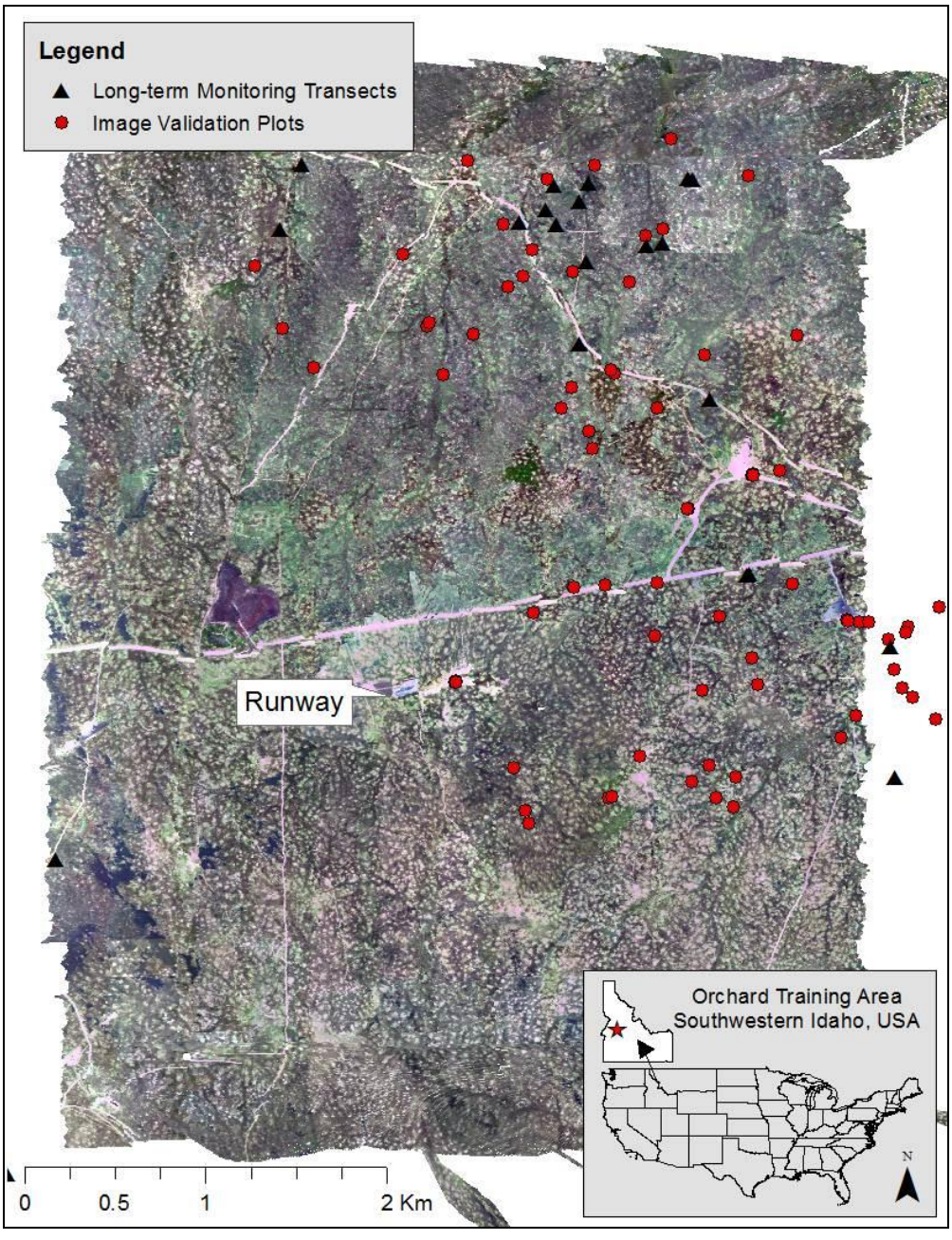

Figure 1. 2011 Hyperspectral coverage (PIKA II) collected in the vicinity of OTA Range 3 Runway. Imagery were obtained from an Arcturus T-16 airframe flying at an elevation of approximately 1676 m above ground level, with a nominal pixel resolution of 1.1 m × 1.1 m.

Prior to mosaicking and classification, flightlines were goeregistered in GeoReg by combining the external orientation data recorded during flight with interior orientation information and a digital elevation model (Hruska et al, 2012). After geocorrections were complete, the flightlines still exhibited a consistent offset of approximately 30 m. To correct for this offset, an optimal set of biases was empirically determined in GeoReg and airframe attitude corrections (roll, pitch, heading: 3, 3.5, 1.25) were applied to the flightlines. Absolute geometric error for the mosaic was assessed using 13 ground control points derived from representative locations throughout corresponding 2009 National Agriculture Imagery Program (NAIP) images (1 m pixel resolution; ± 3 m of Digital Orthophoto Quarter Quad reference maps) and one runway control point collected from a Trimble GeoXT (± 1 m). Absolute geometric error for the mosaic was estimated at having a root mean square error (RMSE) of 7.07 meters.

2.4 Hyperspectral Image Classifications

Unsupervised and supervised classifications were applied to the hyperspectral image mosaic for the purpose of data exploration and land-cover mapping. Unsupervised classifications do not require *a priori* target information and are therefore useful for examining inherent spectral separability among land-cover classes. We selected two commonly used unsupervised algorithms, K-Means and Isodata, to explore the extent to which grass, shrub and bare ground are spectrally distinct in the mosaic.

Supervised classifications were also applied to the image mosaic and included spectral angle mapper (SAM) (Boardman, 1998; Kruse et al, 1993), and the spectral mixture analysis method mixture-tuned matched filtering (MTMF) (Boardman, 1998; Green et al, 1988). A SAM classification was applied to all of the hyperspectral bands and endmember spectra were derived from the mosaic for sagebrush, Sandberg bluegrass, bur buttercup, cinder rock, bare ground and slickspots (Figure 2). Polygon mapping of dense, homogenous targets in the field provided the basis for user-guided endmember pixel selection.

The MTMF method was applied to the hyperspectral mosaic in an attempt to delineate sagebrush cover and estimate subpixel target abundance. A minimum noise fraction (MNF) transformation (Green et al, 1988) was applied to all of the hyperspectral bands and the first 40 MNF bands were retained for MTMF input. Selecting the first 40 bands explained 84% of the data and avoided the introduction of noise associated with higher bands. Sagebrush endmember classification spectra were derived using two different approaches. The first approach used a spectral library of averaged field spectrometer data collected for 35 individual sagebrush canopies at a different study site in eastern Idaho (Mitchell et al, 2012). The second approach used a pixel purity indexing procedure to identify potentially pure pixels in the mosaic for endmember classification. This second approach was eventually dismissed, as the majority of pixels identified by the procedure corresponded to areas of flightline overlap in the mosaic. Further, there was a lack of correspondence between clusters of spectrally pure pixels and known occurrences of sagebrush.

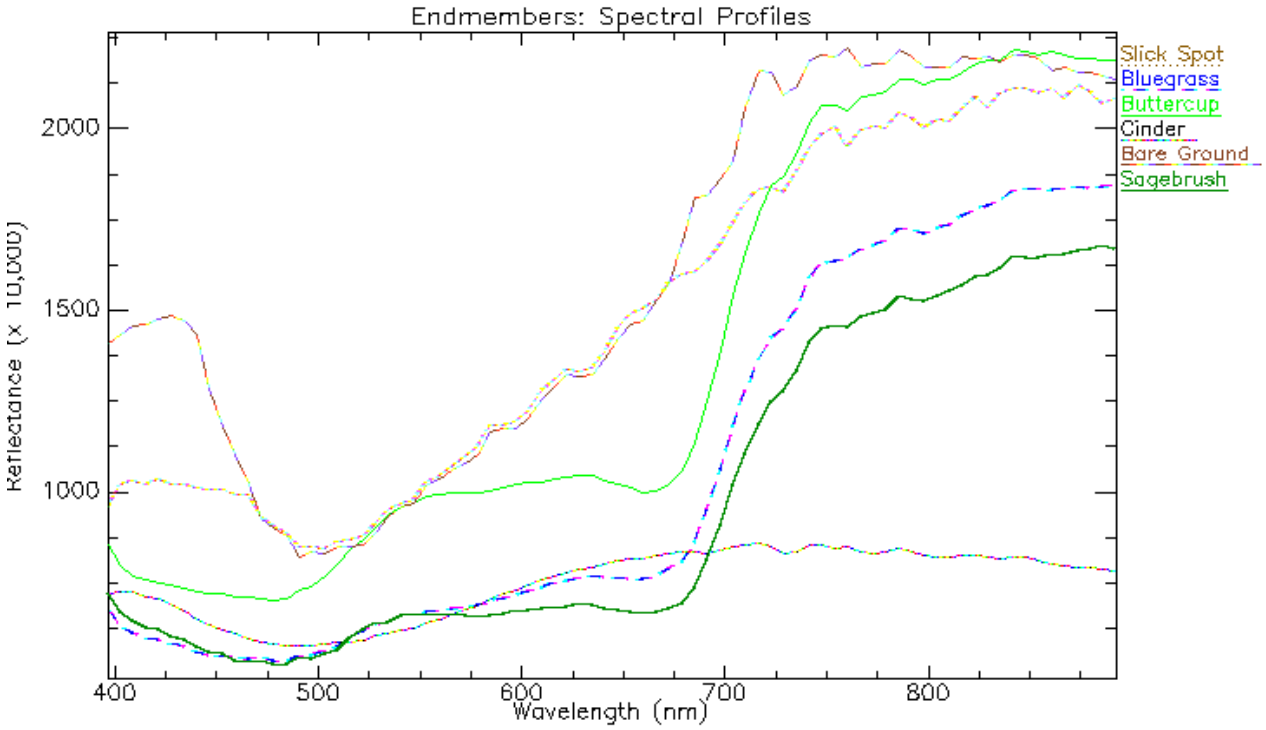

Figure 2. Plot depicting the spectral profiles of image-derived pixel endmembers (slickspots, Sandberg bluegrass, buttercup, cinder, bare ground and sagebrush).

Supervised and unsupervised classification results were qualitatively evaluated based on shrub cover gradients in the study area and visual comparisons to 1) existing OTA vegetation mapping that was developed using a combination of 2012 to 2013 RapidEye (5 m X 5 m) time series imagery and 2012 discrete return light detection and ranging data (lidar) collected by Watershed Sciences, Inc. (now Quantam Spatial) (Spaete et al, 2016) and 2) the ultra-high spatial resolution digital photos that were acquired over the study area during the hyperspectral data collection, and 3) general cover information associated with the 60 sample plots.

In addition to qualitative evaluations, the IsoData classification was quantitatively assessed by generating error matrices and calculating overall accuracy, user's accuracy (percentage of pixels that are correctly classified on the ground), and producer's accuracy (percentage of a given class that is correctly identified on a map).

To quantify the accuracy of the IsoData classification, it was necessary to reclassify the three ground reference categories (shrub, herbaceous and bare ground) into four classes that were spectrally distinct in the classification: shrub, herbaceous, mixed and bare ground. One error matrix was generated using a pixel to plot correspondence, and a second error matrix was generated by applying a 5 m buffer to the plot validation data to conservatively account for geo-registration error in the imagery (Glenn et al, 2005; Williams et al, 2004). Validation plots were classified as "shrub" if the plot contained some combination of 50% to 100% shrub cover and 0% to 50% herbaceous cover. Validation plots were classified as "mixed" if the plot contained any of the following: 25% shrub cover and 25% to 100% herbaceous cover;

or 50% shrub cover and 75% to 100% herbaceous cover; or 75% shrub cover and 75 to 100% herbaceous cover; or and 100% shrub cover and 75% to 100% herbaceous cover. Validation plots were classified as "herbaceous" if the plots contained either of the following: 0% shrub and 50% to 100% herbaceous; or 25% shrub and 100% herbaceous. Finally, validation plots were classified as "bare ground" if the plot contained more than 50% bare ground and 0% vegetation.

3. Results

Evaluation of the mosaicked imagery indicates that increasing flight overlap (176 m), altitude (1676 m AGL) and coarsening the pixel resolution (1.1 m) addressed several issues related to high frequency noise, flight instability and incomplete coverage (Figure 1). Earlier flights conducted at altitudes under 350 m AGL tended to exacerbate flight instability and the pixel size (under 29 x 29 cm) was considered too small to absorb the high frequency error that was evident in the imagery. We empirically determined that increasing flight altitude to above 1500 m, which was permissible at the OTA, coupled with improved flightpath planning (configured for longer approaches to and departures from the flightline) would decrease noise and increase coverage for mosaicking and classification. Compared to earlier flights, lower frequency error in the form of S-shaped flightlines persisted and continued to result in geometric error on the order of 7 m. This error is again attributed to Kalman filters used to predict aircraft position and orientation acquired from a 25 Hz inertial navigation sensor (Hruska et al, 2012). For a description of earlier image acquisitions obtained from an altitude of 305 m (28 cm pixel resolution) see Hruska et al, 2012.

3.1 Unsupervised Classifications

While the K-means unsupervised classification method produced results visually inconsistent with known distribution patterns in the project area, an IsoData classification method (5 classes; minimum class distance of 10 units) produced comparatively similar results to an existing OTA vegetation map (Figure 3). The general sagebrush distribution pattern was consistent between maps, although the mosaic contained a great deal of detail due to the high pixel resolution (1.1 m X 1.1 m). Given the known association between shrubs and shadow, areas in the hyperspectral classification (Figure 3a) that contained shrub with a high degree of shadow mixing appeared to correspond to areas in the current OTA vegetation map (Figure 3b) classified as rabbitbrush.

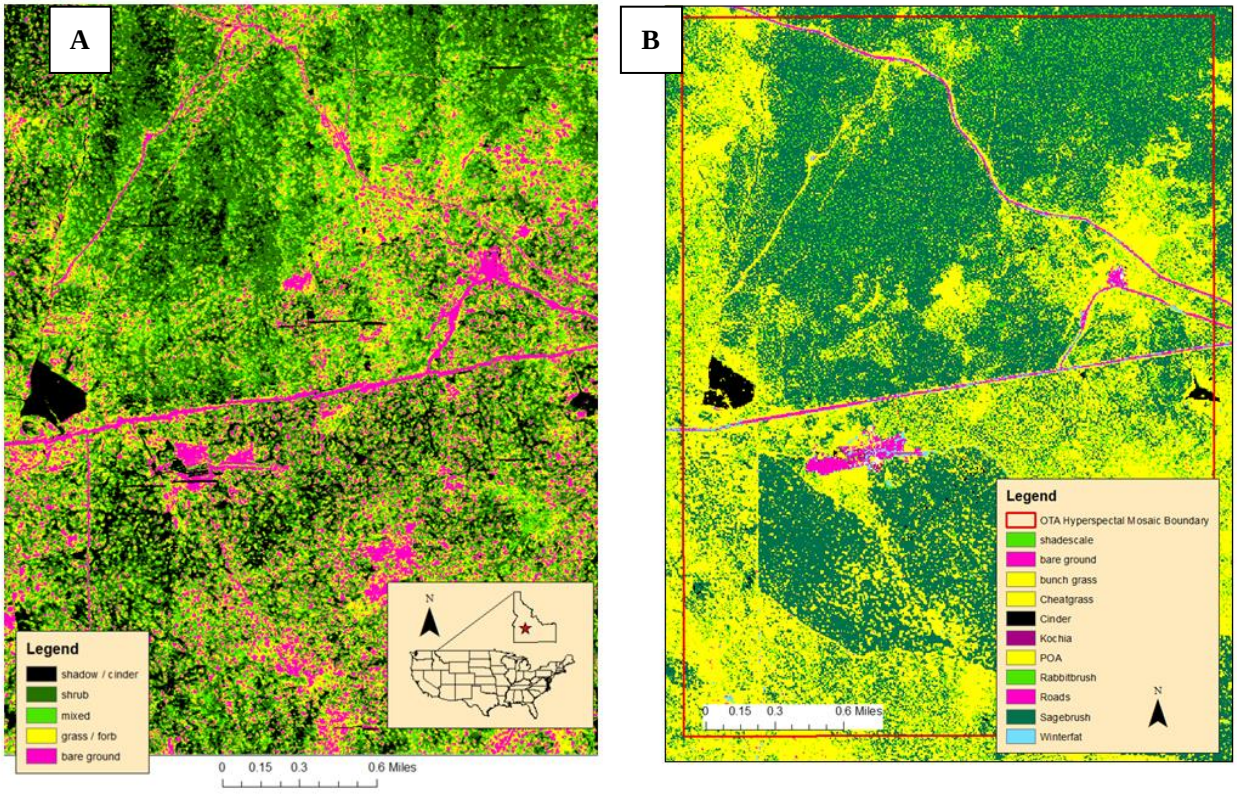

Figure 3. **A**n unsupervised classification (a) was generated from the hyperspectral mosaic, and results were visually compared to a detailed OTA vegetation map (b) derived from year 2014 multi-temporal RapidEye images (Spaete et al, 2016). The general sagebrush distribution pattern is consistent between maps, although the mosaic contains a great deal of detail due to the high pixel resolution (1.1 m X 1.1 m).

Evaluations of the IsoData classification method using several of the ultra-high spatial resolution aerial photographs also suggested reasonable results. For example, areas containing complex distributions of bare ground patches surrounded by grass/forb were validated using the ultra-high resolution aerial photographs (e.g, Figure 4). Differences between the two sets of imagery were attributed to scale: as spectral information is averaged across a coarser pixel resolution (1.1 m) in the hyperspectral mosaic, some signals associated with grass / forb are masked by the brightness of bare ground reflectance and classified as bare ground. The bare ground issue is well documented for dryland ecosystems e.g., (Mitchell et al, 2009) and this classification behavior is expected in portions of the project area where vegetation cover is sparse.

Despite some confusion between grass and bare ground in portions of the project area where cover is sparse, the extent of three isolated slickspot occurrences, located in an area of healthy sagebrush, were mapped correctly in the imagery (Figure 5). Although it is difficult to spectrally distinguish slickspots from other bare ground features such as dirt roads and rocky bare ground, a screening method based on texture and association could be developed to detect potential slickspot occurrences by examining small, isolated patches that are classified as bare ground. Additional comparisons indicated that there is a spectral distinction in the

hyperspectral classification between areas of relatively dense sagebrush cover and areas where shrub cover is lower and the grass / forb understory is more visible to the sensor (Figure 6).

The IsoData accuracy assessment was calculated using 50 of the 60 ground reference plots. Ten of the plots were either outside of the final acquisition area or fell on shadow areas in the classification. The method of using buffered validation data (5 m) to generate error matrices resulted in an overall accuracy of 88%; 0% user's and producer's accuracy in the shrub class; 100% user's and 83% producer's accuracy in the mixed class, 100% user's and 92% producer's accuracy in the herbaceous class; and 50% user's and 100% producer's accuracy in the bare ground class. A conservative and unbuffered version of the same accuracy assessment resulted in an overall accuracy of 28%; 0% user's and producer's accuracy for the shrub class, 50% user's accuracy and 22% producer's accuracy for the mixed class; 47% user's and 32% producer's accuracy for the herbaceous category; and 14% user's accuracy and 50% producer's accuracy for the bare ground class. The low shrub accuracies are influenced by the lack of shrub-dominant validation plots. Studies that have mapped categorical herbaceous and shrub cover categories in the region are large scale (several Landsat scenes) and have obtained shrub cover coefficients ranging from R^2 = 0.28 to R^2 = 0.93 using multi-spatial and –temporal approaches (Homer et al., 2012; Sant et al., 2014).

3.2 Supervised Classifications

The plot of spectral profiles for the image-derived endmember training pixels suggests separability between bare ground, cinder, sagebrush, burr buttercup, and Sandberg bluegrass in the 400 – 900 nm range (Figure 2). While separability between bare ground, cinder and the vegetation targets are visually obvious, it should also be pointed out that, among the vegetation spectra, burr buttercup has an overall brighter reflectance than sagebrush or bluegrass. All three targets have reflectance peaks in the green (~ 550 nm) and red (~ 625 nm) portions of the visible spectrum. The magnitude of green reflectance is the same for both sagebrush and bluegrass. However, sagebrush can be distinguished from bluegrass by a higher reflectance in the red and brighter reflectance along the red edge (~ 725 nm) of the bluegrass spectrum.

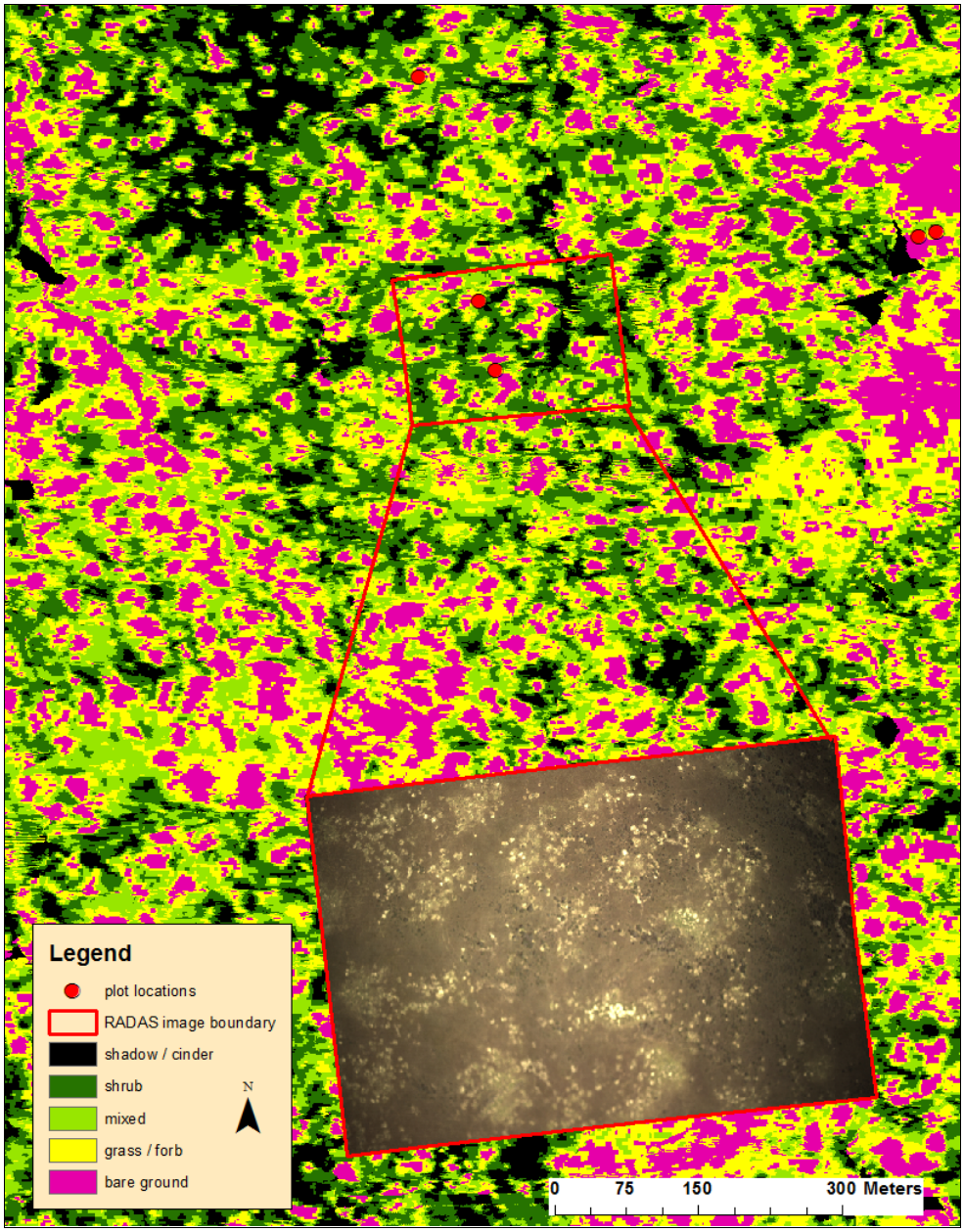

Figure 4. Here the IsoData unsupervised classification method is evaluated for the southeastern portion of the OTA hyperspectral mosaic using an ultrahigh spatial resolution (4.2 cm pixels) image (RADAS) as a basis for comparison. The complex distribution of bare ground patches (magenta) surrounded by grass/forb (light green) is valid based on the ultra-high spatial resolution digital image.

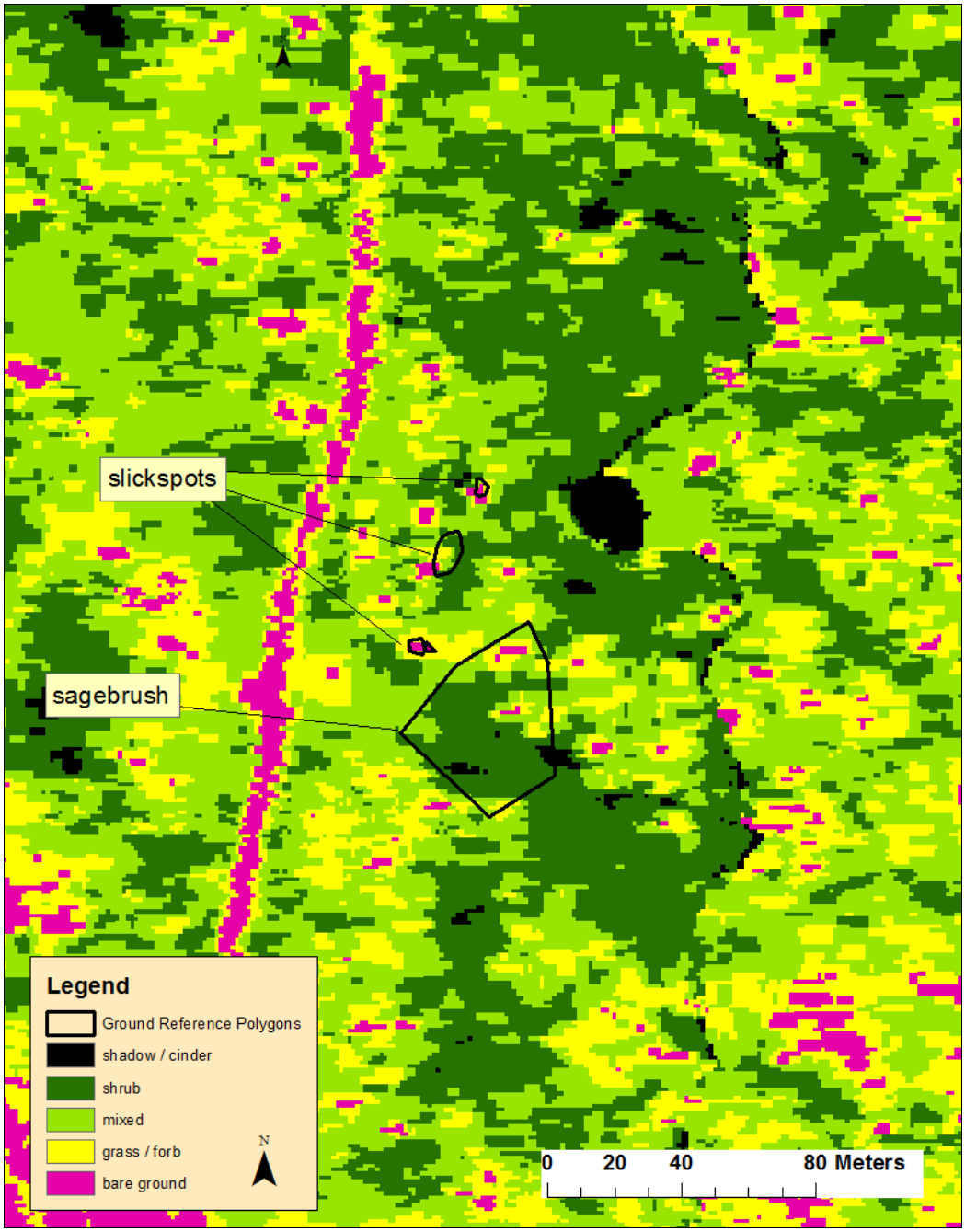

Figure 5. Unsupervised classification performance is evaluated for the central portion of the OTA hyperspectral mosaic using ground reference polygons of slickspot and sagebrush as a basis for comparison. Despite some confusion between grass and bare ground in portions of the project area where cover is sparse, the extent of three isolated slickspot occurrences, located in an area of healthy sagebrush, appear mapped correctly.

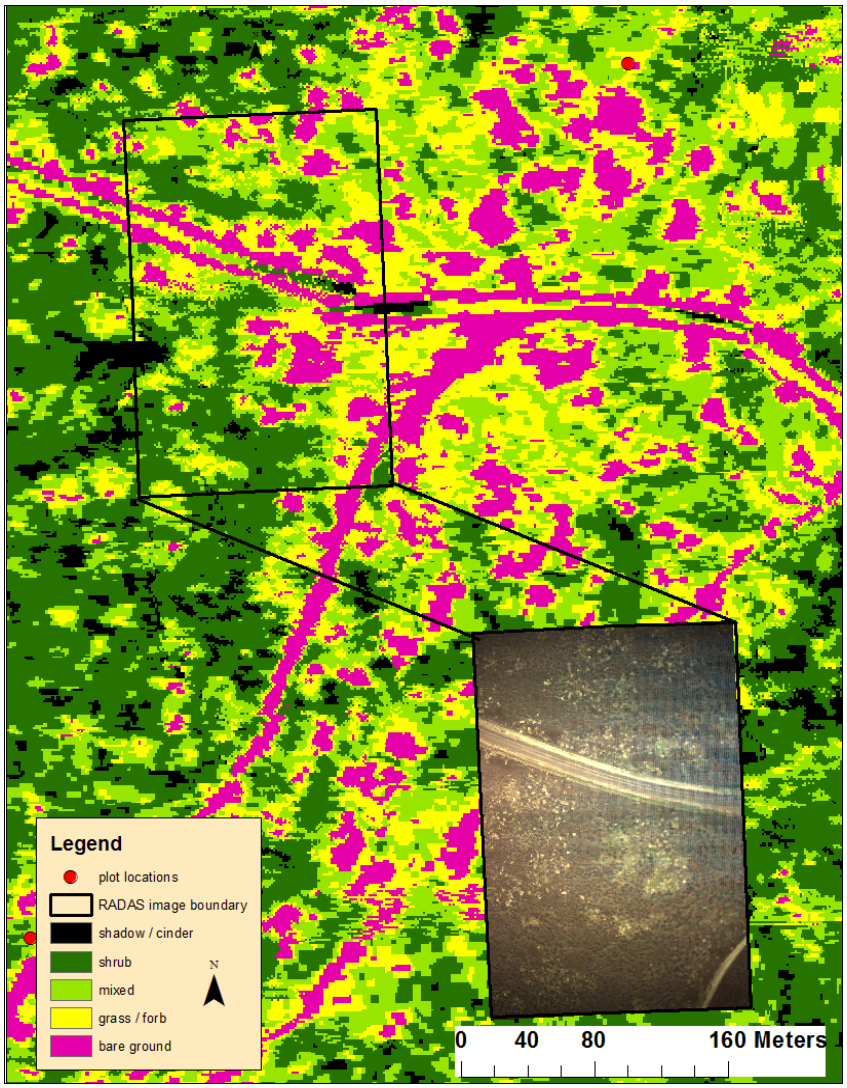

Figure 6. Here the IsoData unsupervised classification method is evaluated for the north-central portion of the OTA hyperspectral mosaic using another RADAS image as the basis for comparison. Mapping results indicate that there is a spectral distinction between areas of relatively dense sagebrush cover (dark green) and areas where shrub cover is lower and the grass / forb understory is more visible to the sensor (light green).

A series of supervised classifications were applied to the hyperspectral mosaic and results were extensively analyzed. All attempts to estimate subpixel target abundance for sagebrush, cinder, bare ground, grass/forb and shadow using an MTMF classification were unsuccessful. Experimentation with sagebrush endmembers derived from a variety of sources (e.g., user-driven, field spectrometer reflectance measurements, ENVI target detection wizard) did not yield a viable map of sagebrush cover. Several other supervised classification methods that were evaluated produced similarly poor results (i.e., including SAM, Constrained Energy Minimization, Orthogonal Subspace Projection and support Vector Machine). The supervised classifications generated results that were not only inconsistent with known sagebrush distribution gradients in the project area, but tended to emphasize either areas of flight overlap and pixel distortion, or areas associated with relatively high reflectance, such as

burrows, mounds and bare ground. This was visually apparent because pixels that were located along flight overlap edges were classified separately from the rest of the image and resulted in an overall corduroy or striped appearance. Comparatively, other airborne hyperspectral studies that have mapped vegetation cover in semi-arid landscapes using an MTMF classification approach have found challenges associated with fine scale heterogeneity (Im et al., 2012) and lack of contrast between target and mixed background (Mitchell et al., 2009). Mundt et al. (2006) used MTMF to classify sagebrush cover with overall accuracies of 74 to 75 percent but had to use a composite endmember that combined two different sagebrush endmember spectra found in the imagery.

4. Discussion and Conclusions

Unmanned Aerial Systems-based hyperspectral test flights at the Orchard Training Area successfully acquired usable flightline data capable of supporting classifiable composite images. Preliminary results of the unsupervised classification support management objectives that rely on mapping shrub cover and distribution patterns of shrubs, herbaceous cover and bare ground.

Overall, supervised classifications performed poorly despite spectral seperability in the image-derived endmember pixels. The MTMF subpixel unmixing algorithm failed to leverage the high spectral dimensionality of the data to estimate sagebrush cover, even though the unsupervised IsoData classification demonstrated spectral distinction between areas of high and low shrub cover. In many cases, the supervised classifications accentuated noise or features in the mosaic that were artifacts of color balancing and feathering areas of flightline overlap. Future supervised classification efforts should focus on endmember derivation and mosaicking procedures and consider a single flightline analysis approach in which the spectral integrity of the data are preserved.

Quantitative accuracy assessments were complicated in this study by high levels of spatial heterogeneity and lens aperture malfunction, which limited the use of ultra-high spatial resolution (RADAS) photos. A quantitative assessment of the IsoData classification produced an overall accuracy as high as 88%, when buffered to allow for geometric error in the hyperspectral mosaic (5 m buffer). The estimation is generous and may benefit from the patchiness of the landscape, which increases the tendency for several different classes to occur within a given buffered field validation point. It is likely that the collection of additional ground reference data, including extensive training polygons, would improve classification performance. Future mapping efforts that minimize geometric error, leverage ground reference data, maximize flight planning to avoid pixel distortion and minimize illumination differences between flightlines, and time series analysis should be able to effectively distinguish native grasses, invasives and shrubs using the higher reflectance spectrum of the burr buttercup and the higher peak in the red and along the red edge of the bluegrass.

Acknowledgement

This project was made possible by Nick Nydegger (GIS Systems Manager) and Charles Baun

(Conservation Branch Manager) of the State of Idaho, Military Division of the Idaho Army National Guard. Both provided strategic mission input, coordinated use of airspace and provided ground access to the Orchard Training Area project area. The authors would also like to thank Anna Halford (Botanist, Morley Nelson Snake River Birds of Prey National Conservation Area), of the Bureau of Land Management (BLM), who assisted in identifying conservation applications in the field. Finally, thanks to Jay Weaver of the Idaho Army National Guard, Jayson Murgoitio of the BLM Boise Idaho (then graduate student at BCAL) and Lucas Spaete (Research Assistant) of BCAL for their assistance in collecting ground reference data in the field.

References

Anderson, K., & Gaston, K. J. (2013). Lightweight unmanned aerial vehicles will revolutionize spatial ecology. *Frontiers in Ecology and the Environment, 11*, 138-146. http://dx.doi.org/10.1890/120150

Boardman, J. W. (1998). Leveraging the high dimensionality of AVIRIS data for improved sub-pixel target unmixing and rejection of false positives: mixture tuned matched filtering, Summaries of the Seventh JPL Airborne Earth Science Workshop, NASA Jet Propulsion Laboratory, Pasadena, CA, USA, pp. 55-56.

Duan, S. B., Li, Z. L., Wu, H., Tang, B. H., Ma, L., Zhao, & E., Li, C. (2014). Inversion of the PROSAIL model to estimate leaf area index of maize, potato, and sunflower fields from unmanned aerial vehicle hyperspectral data, *International Journal of Applied Earth Observation and Geoinformation, 26*, 12-20. http://dx.doi.org/10.1016/j.jag.2013.05.007

Green, A. A., Berman, M., Switzer, P., & Craig, M. D. (1988). A transformation for ordering multispectral data in terms of image quality with implications for noise removal, *IEEE Transactions on Geoscience and Remote Sensing, 26*, 65-74. http://dx.doi.org/10.1109/36.3001

Glenn, N., Mundt, J., Weber, K., Prather, T., Lass, L., & Pettingill, J. (2005). Hyperspectral Data Processing for Repeat Detection of Small Infestations of Leafy Spurge, *Remote Sensing of Environment, 3*, 399-412. http://dx.doi.org/10.1016/j.rse.2005.01.003

Hardin, P. J., & Jackson, M. W. (2005). An unmanned aerial vehicle for rangeland photography, *Rangeland Ecology and Management, 58*, 439-442. Doi:10.2111/1551-5028(2005)058

Hardin, P. J., & Jensen, R. R. (2011). Small-scale unmanned aerial vehicles in environmental remote sensing: Challenges and opportunities. *GIScience & Remote Sensing, 48*, 99-111. http://dx.doi.org/10.2747/1548-1603.48.1.99

Hruska, R., Mitchell, J., Anderson, M., Glenn, N, Halford, A, & Baun, C. (2014). Radiometric and geometric analysis of hyperspectral imagery acquired from an Unmanned Aerial Vehicle (UAV), *Remote Sensing, 2012, 4*, 2736-2752. http://dx.doi.org/10.3390/rs4092736

Im, J., Jensen, J. R., Jensen, R. R., Gladden, J., Waugh, J., & Serrato, M. (2012). Vegetation cover analysis of hazardous waste sites in Utah and Arizona using hyperspectral remote sensing. *Remote Sensing, 4*, 327-353. http://dx.doi.org/10.3390/rs4020327

Laliberte, A. S., & Rango, A. (2009). Texture and scale in object-based analysis of sub-decimeter resolution unmanned aerial vehicle (UAV) imagery, *IEEE Transactions on Geoscience and Remote Sensing, 47*, 761-770. http://dx.doi.org/10.1109/TGRS.2008.2009355

Laliberte, A. S., Goforth, M. A., Steele, C. M., 7 Rango, A. (2011). Multispectral remote sensing from unmanned aircraft: Image processing workflows and applications for rangeland environments, *Remote Sensing, 3*, 2529-2551. http://dx.doi.org/10.3390/rs3112529

Lucieer, A., Malenovský, Z., Veness, T., & Wallace, L. (2014). HyperUAS-Imaging spectroscopy from a multirotor unmanned aircraft system, *Journal of Field Robotics, 31*, 571-590. http://dx.doi.org/10.1002/rob.21508

Michez, A., Piégay, H., Lisein, J., Claessens, H., & Lejeune, P. (2016). Classification of riparian forest species and health condition using multi-temporal and hyperspatial imagery from unmanned aerial system, *Environmental Monitoring and Assessment, 188*, 1-19. http://dx.doi.org/10.1007/s10661-015-4996-2

Mitchell, J., & Glenn, N. (2009). Leafy spurge (Euphorbia esula L.) classification performance using hyperspectral and multispectral sensors, *Rangeland Ecology and. Management, 62*, 16-27. http://dx.doi.org/10.2111/08-100

Mitchell, J., Glenn, N., Sankey, T., Derryberry, D., Anderson, M., & Hruska, R. (2012). Spectroscopic detection of Nitrogen concentrations in sagebrush: implications for hyperspectral remote sensing, *Remote Sensing Letters, 3*, 285-294. http://dx.doi.org/10.1080/01431161.2011.580017

Mundt, J. T., Streutker, D. R., & Glenn, N. F. (2006). Mapping sagebrush distribution using fusion of hyperspectral and lidar classifications. *Photogrammetric Engineering & Remote Sensing, 72*, 47-54. http://dx.doi.org/10.14358/PERS.72.1.47

Okin, G. S., Roberts, D. A., Murray, B., & Okin, W. J. (2001). Practical limits on hyperspectral vegetation discrimination in arid and semiarid environments, *Remote Sensing of Environment, 77*, 212-225. http://dx.doi.org/10.1016/S0034-4257(01)00207-3

Puliti, S., Ørka, H. O., Gobakken, T., & Næsset, E. (2015). Inventory of small forest areas using an unmanned aerial system. *Remote Sensing, 7*, 9632-9654. http://dx.doi.org/10.3390/rs70809632

Sant, E. D., Simonds, G. E., Ramsey, R. D., & Larsen, R. T. (2014). Assessment of sagebrush cover using remote sensing at multiple spatial and temporal scales. *Ecological Indicators, 43*, 297-305. http://dx.doi.org/10.1016/j.ecolind.2014.03.014

Spaete, Lucas P.; Glenn, Nancy F.; and Baun, Charles W. (2016). *Morley Nelson Snake River Birds of Prey National Conservation Area 2013 RapidEye 7m Landcover Classification* [Data set]. Boise, ID: http://dx.doi.org/10.18122/B21592

Suomalainen, J., Anders, N., Iqbal S., Roerink, G., Franke, J., Wenting, P., Hünniger D., Bartholomeus, H., Becker, R., & Kooistra, L., (2014). A Lightweight Hyperspectral Mapping System and Photogrammetric Processing Chain for Unmanned Aerial Vehicles, *Remote Sensing*, *6*, 11013-11030. http://dx.doi.org/10.3390/rs61111013

Uto, K., Seki, H., Saito, G, & Kosugi, Y. (2013). Characterization of Rice Paddies by a UAV-Mounted Miniature Hyperspectral Sensor System, *IEEE Journal of Selected Topics in Applied Earth Observations and Remote Sensing*, *6*, 851-860. http://dx.doi.org/10.1109/JSTARS.2013.2250921

Wallace, L., Lucieer, A., & Watson, C. S. (2014). Evaluating tree detection and segmentation routines on very high resolution UAV LiDAR data. Geoscience and Remote Sensing, *IEEE Transactions on, 52*, 7619-7628. http://dx.doi.org/10.1109/TGRS.2014.2315649

Zarco-Tejada, P. J., Catalina, A., González, M. R., & Martín, P. (2013). Relationships between net photosynthesis and steady-state chlorophyll fluorescence retrieved from airborne hyperspectral imagery. *Remote Sensing of Environment*, *136*, 247-258. http://dx.doi.org/10.1016/j.rse.2013.05.011

Copyright Disclaimer